Scanning Microscopy

Volume 1990
Number 4 *Fundamental Electron and Ion Beam Interactions with Solids for Microscopy, Microanalysis, and Microlithography*

Article 12

1990

Murphy's Law and the Uncertainty of Electron Probes

Linn W. Hobbs
Massachusetts Institute of Technology

Scanning Microscopy Supplement 4, 1990 (Pages 171-183) 0892-953X/90$3.00+.00
Scanning Microscopy International, Chicago (AMF O'Hare), IL 60666 USA

MURPHY'S LAW AND THE UNCERTAINTY OF ELECTRON PROBES

Linn W. Hobbs

Room 13-4062,
Massachusetts Institute of Technology,
Cambridge, MA 02139, U.S.A.

Phone: (617) 253-6835

Abstract

The electron microscope has brought over the last fifty years a wealth of information about the structure of solids, from surface topography to the details of atomic arrangements. Like any probe, however, the electron beam is subject to the epistomological constraint that the investigator inevitably perturbs what is being investigated, and from its beginnings questions were raised about the integrity of the images generated in the microscope from a specimen which was subjected to such an aggressive probe. A fast electron is about as likely to be scattered inelastically as elastically from a collection of atoms, and the density of energy transfer to these atoms, under conditions where their positions or identities can be established, approaches that in a modest nuclear explosion. It is, indeed, a tribute to the redundancy of atomic bonding in solids that atomic organization is largely maintained during investigation. It was early recognized that biological solids were substantially affected; only recently has it been realized that the integrity of atomic-scale information from inorganic solids as well can be seriously compromised by the investigating electron. This contribution reviews the interaction modes which are relevant to the deterioration of specimens in a fast electron beam, outlines the mechanisms by which these interactions lead to irreversible alterations in structure, and assesses the rates at which these alterations proceed in the several instrumental configurations of the electron microscope represented by the scanning electron microscope (SEM), conventional transmission electron microscope (CTEM), and scanning transmission electron microscope (STEM). Incidences of degradation are illustrated for investigation of several structural classes, and several palliative measures are described.

Key Words: Electron irradiation damage, electron beam heating, specimen charging, radiolysis, electron-stimulated desorption, atom displacement rates, damage kinetics and temperature dependence, minimum dose microscopy.

Introduction

The making of any physical measurement is necessarily accompanied by two unwelcome but fundamental features: uncertainty and perversity. The first represents a limitation deriving from immutable laws governing the functioning of our universe, while the second is the anthropomorphic embodiment of our inability to accept the limitations imposed by the first. Uncertainty is commonly expressed by the formulation of Heisenberg (in 1927) which establishes quantifiable uncertainties δ inherent in the joint measurement of certain pairs of attributes, e.g. position x and momentum p_x

$$\delta x \cdot \delta p_x \geq h \qquad (1)$$

The restriction imposed by (1) can easily be shown to govern the positional resolution δx of any imaging system which employs a probe, such as an electron or photon, a change in whose momentum δp_x upon interaction with the matter to be imaged forms the basis for image contrast (Fig. 1). Such a probe may be assigned a wavelength λ and wave vector $k = 1/\lambda$ via the de Broglie relation

$$|p| = h/\lambda = |hk| \qquad (2)$$

If the interaction deflects the propagation direction of the probe through an angle θ, the change in momentum is given by

$$\delta p_x = \pm\, h\, \delta k = 2\, hk \sin\theta$$

whence (1) can be rewritten

$$\delta x \geq 1/(2\, k \sin\theta) = \lambda/(2 \sin\theta) \qquad (3)$$

which is the familiar diffraction-imposed resolution limit.

The notion of perversity is popularly personified in the fatalistic law introduced by Murphy (1949)

"If anything can go wrong, it will!" (4)

illustrated empirically by its more familiar consequences, such as that buttered toast always falls butter-side down on the new carpet, or by appeal to its variant

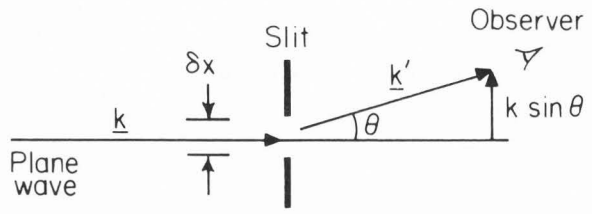

Fig. 1. Diffraction limit for resolution derived from the de Broglie relationship and Heisenberg's Uncertainty Principle.

"You can't tell how deep a puddle is until you step in it." (5)

The corollative statement (5) is nothing more than a restatement of the Heisenberg Uncertainty Principle (1), which in its consequential formulation holds that, by the act of imposing measure, the measurer inevitably perturbs that which is being measured and so introduces the requisite uncertainty.

It is in this sense that the present paper will address the issues of uncertainty and perversity in the use of electron probes for the investigation of structure and composition, with particular reference to use of the electron microscope in its imaging and analytical modes.

Table of Symbols

a_H	Bohr radius of hydrogen atom (53 pm)
A	materials constant for high-current conduction ($\sim 10^{-3}$ $\sqrt{(V/m)}$)
b	radius of electron-illuminated area (m)
c	speed of light (3×10^8 m/s)
c	defect concentration or damage fraction
c_d	fraction of atoms displaced, or displacements per atom (dpa)
c_d	fraction of atoms displaced per unit time (dpa s^{-1})
C	analytical signal event count
d	image resolution (m)
dU/dz	electron stopping power (J/m, eV/m)
D	electron fluence or dose (electrons/m^2)
e	electron charge (1.6×10^{-19} C)
E	(radial) electric field
E*	(radial) electric field for specimen foil at steady-state charge
G	forward rate of primary damage events (m^2/electron)
G'	production rate of defect fraction surviving recombination or restoration (m^2/electron)
h	Planck's constant (6.6×10^{-34} J s)
i	incident electron current (A)
i_c	specimen conduction current
i_s	secondary electron emission current
j	incident electron current density (A/m^2)
j_c	specimen conduction current density (A/m^2)
j_o	high-field conduction current density (A/m^2)
k	electron wave vector (m^{-1})
k_B	Boltzmann constant (1.38×10^{-23} J/K)
m	electron mass
m'	multiplicity of damage events required for permanent damage
M	nuclear mass (kg)
N	atom density in specimen (m^{-3})
N_e	density of valence electrons in specimen (m^{-3})
p	electron momentum (kg•m/s)
R	fractional rate of damage restoration (m^2/electron)
R'	initial rate of damage restoration at zero defect fraction (m^2/electron)
R"	rate of non-geminate athermal restoration (m^2/electron)
t	specimen foil thickness
T	specimen temperature
U	incident electron energy (J, keV)
U_R	Rydberg energy (13.6 eV)
U_{th}	threshold energy for incident electrons to inititate knock-on atom displacements (J, keV)
V*	potential of specimen foil acquiring steady-state charge (V)
W	secondary electron energy (J)
W*	electron energy at potential V* (J)
x	spatial position (m)
Z	atomic number
α	angular deflection of incident electron beams (rad)
β	efficiency of signal collection ($0<\beta<1$)
γ	image contrast ($0<\gamma<1$)
δx	uncertainty in position (m)
δp	uncertainty in momentum (kg•m/s)
ΔT	specimen temperature rise (K)
ϵ_o	electrical permittivity of vacuum (8.85×10^{-12} F/m)
ζ	efficiency of radiolytic displacement process ($0<\zeta<1$)
η	multiplicity factor for signal generation ($0<\eta$)
Θ	electron diffraction angle (rad)
κ	specimen thermal conductivity (W/m•K)
λ	electron wavelength (m)
σ_d	cross-section for knock-on atom displacement (m^2, barns)
σ_c	electron-electron inelastic interaction cross-section (m^2, barns)
σ_i	cross-section for inelastic process generating analytical signal (m^2, barns)
σ_n	electron-nucleus inelastic interaction cross-section (m^2, barns)
σ_r	cross-section for radiolytic atom displacement (m^2, barns)
$\sigma(W>W*)$	cross-section for emission of secondary electrons with energies W>W* (m^2, barns)
τ_d	kinetic energy transfer required for atomic displacement (J,eV)
τ_e	energy transferred in electron-electron collision (J, eV)
τ_n	energy transferred in electron-nucleus collision (J, eV)
ω	athermal recombination volume (m^3, atomic volumes)

Electrons for Imaging and Analysis

High energy (> 10 keV) electron beams are among our most sensitive probes for structure of solid materials and the most spatially specific. Information about surface and internal structure is routinely obtained at the atomic level with the conventional transmission electron microscope (CTEM) using elastically forward-scattered electrons; about elemental composition on a near-atomic scale with the scanning transmission electron microscope (STEM) using inelastically-scattered electrons (electron energy-loss spectroscopy, or EELS) and the X-rays they generate (X-ray energy dispersive spectroscopy, or XEDS); and about surface morphology on a 1 nm scale with the scanning electron microscope (SEM) using secondary and backscattered electrons. Electron probes are unfortunately not entirely benign, in that their very interaction with the matter under examination--which interaction is responsible for the signal being measured--inevitably disturbs the subject studied in some not insignificant ways. This situation is simply the Uncertainty Principle writ large, as suggested above: the investigator inescapably perturbs his experiment. To the extent that the structural organization of the matter investigated is irrecovably altered during its interaction with the electron beam, any information we derive must be considered suspect, and the specimen is said to sustain "radiation damage." That this is **generally** the case is not widely appreciated (Hobbs, 1984), though the possibility of electron irradiation damage may be admitted in specific instances where its effects are undeniably apparent.

The formation of an electron image and the collection of an analytical signal are statistical processes to which Poisson statistics apply. The minimum electron dose (fluence) D required to image an object feature with resolution d exhibiting contrast $\gamma < 1$ is given by the Rose (1948) criterion, developed originally for television

$$D > k^2/(d^2\gamma^2\eta\beta) \qquad (6)$$

where k is a signal/noise ratio (typically > 5) required for recognition of detail, η is the multiplicity of signal generation and $\beta < 1$ is the efficiency of signal collection. For CTEM, where forward-scattered electrons are collected, nearly all incident electrons are transmitted; however, no more than half of the incident electrons are either elastically scattered or (in thicker specimens) inelastically scattered and still preserve contrast, so $\eta < 0.5$. The collection efficiency for recording in photographic emulsions is close to unity (Valentine, 1965), but $\eta \simeq 0.1$ because the objective aperture (or effective pupil set by chromatic aberration and partial coherence) subtends only a portion of the solid angle through which electrons are scattered. For atomic scale images ($d \simeq 0.1$ nm) of necessarily very thin (10 nm) specimens, perhaps 80% of incident electrons remain unscattered; of the scattered 20%, possibly less than half are within the objective lens pupil function, so again, $\eta \simeq 0.1$, and such images require $D > 10^6$ e/nm^2 on this criterion. For STEM, η is closer to unity (in thicker specimens, because both elastically and inelastically scattered electrons can be made to contribute to the image signal) and β is larger than for CTEM because of the greater collection efficiency of the larger dark-field detector. For SEM modes in which primarily secondary electrons are collected, $\eta < 1$ is the secondary yield and $\beta \leq 1$ is their collection efficiency by the secondary electron detector. At the 1 nm resolution level, set by beam broadening in the semi-infinite specimens used in SEM for which $\eta \simeq 0.1$ (Schou, 1988) and $\beta \simeq 0.5$, a dose $D > 1000$ e/nm^2 is necessary.

The requirements of microanalysis (EELS, XEDS) are analogous. The number of counts C detected for some particular inelastic process (electron energy loss, X-ray emission) with cross section σ_i from N atoms is

$$C = D\ N\ \sigma_i\ \beta; \qquad (7)$$

for 10% counting statistics, C = 100. The minimum electron dose required to detect N atoms is therefore

$$D > 100/(N\ \sigma_i\ \beta) \qquad (8)$$

which, for typical values of N and σ_i, yields a best case $D > 10^6$ e/nm^2 to detect single atoms, and in most instances much higher required doses. Table 1 summarizes these results for common imaging and analytical instrument modes. Both (6) and (8) are fundamental limitations and cannot be improved upon by any instrument configuration.

Table 1

Electron Dose Required for 'Atomic' Information

TEM	Structure image	1×10^6 e/nm^2
STEM	Dark-field image	2×10^5
SEM	Secondary image	1×10^5
EELS	Valence excitation	2×10^6
EELS	Oxygen K edge (25 eV window, 10 mrad detector)	3×10^9
XEDS	Iron K_α	4×10^{11}

Elastic and Inelastic Interactions

The coulombic interaction of a fast electron and an atom can be considered as truly **elastic** only if no energy is dissipated in the interaction, which in a solid can occur only when quantum considerations proscribe momentum transfers to the individual components of the solid (electrons, nuclei) and the solid as a whole recoils. Since the latter is so massive, the incident electron loses negligible kinetic energy (**zero loss**). Elastic scattering occurs predominantly in the forward direction with a mean-free path between collisions of order 100 nm. **Inelastic** scattering redistributes the recoil kinetic energy into internal energy of the solid. Quantum proscriptions confine such energy transfers to well-defined transitions between

quantum states--phonon states for nuclei; atomic electron energy levels, energy bands or collective modes for the associated electrons--with mean-free paths between interactions for the most common excitations (phonons; collective valence electron excitations called plasmons) also of order 100 nm. A fast electron (kinetic energy U > 10 keV) is therefore at least as likely to be inelastically as elastically scattered and, for specimen thicknesses of 100 nm or more, much more likely to be scattered than not (see Kohl, 1990).

Of those incident electrons scattered **inelastically**, an estimate of the ratio of those interacting inelastically with electrons (mass m) and those interacting inelastically with nuclei (mass M, atomic number Z) can be obtained from the respective interaction cross sections (Hobbs, 1984) in their non-relativistic form

$$\sigma_e \simeq (4\pi\ a_H^2 U_R^2)\ Z/(U\ \tau_e^{min}) \qquad (9)$$

$$\sigma_n \simeq (4\pi\ a_H^2 U_R^2)\ (Z^2\ m/M)/(U\ \tau_n^{min}) \qquad (10)$$

where a_H = 0.053 nm is the Bohr radius of a hydrogen atom; U_R = 13.6 eV is the Rydberg energy; and $\tau_e^{min} \simeq$ 2 eV and $\tau_n^{min} \simeq k_B T \simeq 0.02$ eV are the minimum average kinetic energies respectively transferrable to electrons and nuclei in the quantized solid. The ratio of these cross sections

$$\sigma_e/\sigma_n = (M/mZ)\ \tau_n^{min}/\tau_e^{min} \simeq 40 \qquad (11)$$

reveals that inelastic interaction with atomic electrons always predominates over inelastic interaction with nuclei.

The average **rate** of energy loss (per unit path length) to electronic processes (and thus the approximate overall energy loss rate) in a solid with atom density N can be obtained from (10) as the familiar Thomson-Whiddington law (Whiddington, 1914)

$$-dU/dz \simeq (4\pi\ a_H^2 U_R^2)\ N\ Z\ (1/U)\ \ln(U/\tau_e^{min}) \qquad (12)$$

The **stopping power** dU/dz is essentially constant over thickness of TEM or STEM specimens and over the thickness in SEM specimens from which secondary electrons are emitted and typically varies from ~10^{10} eV/m for U = 10 keV to ~10^8 eV/m for U = 1 MeV (Spencer, 1959). Electron currents in TEM probes are very small, typically i $\simeq$ 1 - 100 nA, but the current densities must be very high, j $\simeq$ 10^4 - 10^6 A/m^2 for resolution of atomic-scale information, requiring informative electron doses D > 10^6 e/nm^2 acquired over 1-10 s collection times. Because at least 10% of the incident electrons are inelastically scattered in 10 nm-thick specimens (more like half in thicker specimens), we may assume that at least 10% of this dose contributes to energy deposition in the specimen at a rate of 10^8 - 10^{10} eV/m per electron, or an overall energy deposition rate of 1-100 kW/mm^3. These rates are comparable to that of a modest thermonuclear explosion a few tens of meters from the epicenter. Viewed from this perspective, it is surprising that specimens are not more altered than appears to be the case.

Charging and Heating

Two immediate consequences of the inelastic interactions are charge acquisition by the specimen and specimen heating. Specimen charging occurs when the flux of incident electrons thermalized inside the specimen is not balanced by the flux of electrons leaving the specimen by forward- or back-scattering elastic interactions or from secondary electron emission. This subject is considered in detail by Cazaux and LeGressus (1991) for the case of solid specimens in SEM, for which case the majority of incident electrons are thermalized inside the specimen and the specimen usually acquires a **negative** charge (β < 1).

The case of thin TEM specimens is very different because essentially all of the electrons incident on one face of the specimen emerge from the other, and it is the emission of secondary electrons from both faces which makes the specimen acquire a **positive** charge. If uncompensated by a current of electrons conducted into the irradiated area from the surroundings, this charge will elevate the specimen potential, which in turn will both throttle further secondary emission and drive insulating specimens into non-ohmic conduction regimes, leading to electrical discharge breakdown. Semiconduction is adequate to avoid this regime, but insulators require special treatment.

A more quantitative estimate of the problem for insulators can be approached as follows (Hobbs, 1974). A positive foil potential V* prevents secondary electrons of energy W < W* = V*e from leaving the foil. The range of even the most probable secondaries (W $\simeq$ 10 eV) is of the order of the foil thickness t, so that the secondary emission current, made up of all secondaries with energies W > W*, is given by

$$i_s \simeq i\ N_e\ t\ \sigma(W > W^*) \qquad (13)$$

where N_e is the density of valence electrons and the total cross section $\sigma(W > W^*)$ for production of secondary electrons of energy W > W* is approximately (Mott and Massey, 1965)

$$\sigma(W > W^*) \simeq \pi e^4/(4\pi\epsilon_o)W^*U = e^3/4\epsilon_o V^*U$$

provided 10 volts < V* < U/e. The corresponding (radial) electric field E* will be maximum at the periphery of the irradiated area of radius b

$$E^*(max) = V^*/b \qquad (14)$$

or about 10^6 V* V/m for b $\simeq$ 1 μm.

Conduction becomes non-ohmic for most insulators for E > 10^6 V/m, so even a small foil potential V* will induce field-dependent conductivity. The conduction current density j_c can be described in this regime by

$$j_c = j_o \exp A\sqrt{E}$$

where $j_o \simeq 10^{-13}$ A/m^2, the high-field conduction extrapolated to zero field, and A $\simeq 10^{-3}\ \sqrt{(V/m)}$ are materials constants. The conduction current i_c is thus

$$i_c = 2\pi\ b\ t\ j_o \exp A\sqrt{(V^*/b)}. \qquad (15)$$

Setting i_c equal to i_s,

$$V^* \exp A\sqrt{(V^*/b)} = e^3\ i\ N_e/(4\pi\ \epsilon_o\ A\ U) \qquad (16)$$

whence V* can be obtained. For i = 1 nA and U = 100 keV, (16) yields

$$V^* \simeq 350 \text{ V}$$

$$E^* \simeq 3 \times 10^8 \text{ V/m}.$$

This value of E is of the order of dielectric strengths of insulators, and breakdown can clearly occur. Attraction of secondary electrons emitted from other surfaces, such as the nearby objective aperture, is important in this regime as a source of additional electron current and will influence V*. Nevertheless, V* cannot fall below the threshold for emission from the surrounding metal surfaces (5-10 eV) which is larger than for emission from most insulators (~ 0.5 eV), so a large field, E ~ 10^7 V/m will still be sustained.

From the standpoint of electron optics, the difficulty is the consequent electric field sustained between the positively-charged specimen and its near surroundings (specimen holder, objective aperture) which is strong enough to act as an electrostatic lens introducing unacceptable image distortions and lateral beam shifts. The magnitude of beam deflection is given by

$$\alpha \simeq (e/U)\int_b^t (V^*/z)dz = (V^* e/U)\ \ln(t/b) \qquad (17)$$

assuming that the net transverse field is of the same order of magnitude as the radial field (14). For U = 100 keV and V* = 100 V, (17) yields $\alpha \simeq 10$ mrad, or about a Bragg angle, which is approximately what is observed. A simple remedy for insulators is to coat the specimen with a thin conducting film of low atomic number material, e.g. evaporated C or Al, which makes electrical contact to the metallic specimen holder. This film must be thick enough (> 10 nm) to be continuous, but need coat only **one** side (the exit side is best) to eliminate the perturbing **external** electric field otherwise generated; the **internal** field remaining in the specimen does not act over a sufficiently large distance to be troublesome for imaging. Nevertheless, possible effects of strong internal electric fields on the specimen should not be discounted. A further discussion of this point can be found in the contribution by Cazaux and Le Gressus (1990).

Heating is a second consequence of the electron energy deposited in the specimen. Assuming that the major portion of the electron energy loss ends up as heat, the consequent elevation of specimen temperature depends critically on the available thermal conduction paths to the cooler surroundings. The temperature rise can be calculated by solving the radial form of the differential equation for heat conduction

$$(1/r)\ \partial(r\ \partial T/\partial r)/\partial r + j\ (dU/dz)/(\kappa\ e) = 0 \qquad (18)$$

for the appropriate boundary conditions; the important parameters are the time rate of heat input per unit volume j (dU/dz)/e at radius r and the specimen thermal conductivity κ. For most TEM specimen geometries, the resulting temperature rise is (Hobbs, 1984)

$$\Delta T = i\ [(dU/dz)/2\pi\ e\ \kappa)][1/2 + 2\ \ln(c/b)] \qquad (19)$$

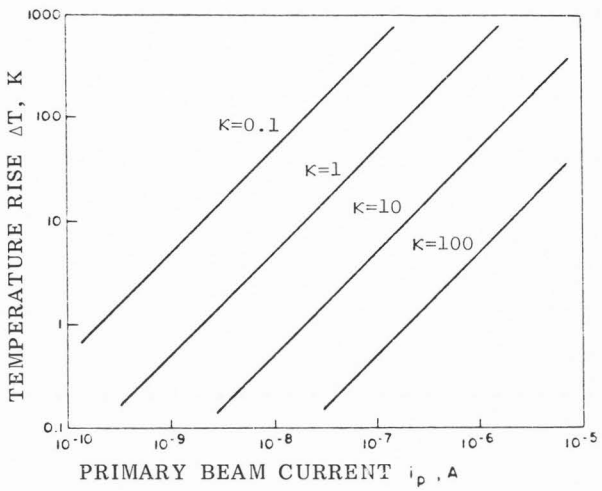

Fig. 2. Specimen temperature rise for TEM specimens as a function of total electron beam current and thermal conductivity κ (in W/m·K) assuming a good thermal sink.

where c is a geometrical constant of at most the specimen radius. (For example, $c^2 = b\sqrt{(\rho t)}$ for dish-polished specimen geometries, where ρ is the radius of polishing curvature; for flat specimen geometries, c is the distance to the nearest thermal sink). The specimen thermal conductivity κ can vary from 0.1 W/m·K for poor conductors (like ceramics or carbon films) to 100 W/m·K for metals. It is important to note that the temperature rise is, to first order, proportional to the total beam **current** i, not the **current density** j, so that spreading the beam or spreading the probe size with the condensor lens has little effect. Expected temperature rises are plotted in Fig. 2, assuming that the specimen is adequately fixed to a good thermal sink. The heating effect is negligible ($\Delta T < 10$ K) for most materials and moderate beam currents and troublesome only for very poor thermal conductors under high beam currents or when thermal contact to a sink is inadequate. Ceramic powders simply lying on carbon films are particular offenders, and temperatures high enough to induce melting may be sustained in them. In SEM, where the entire kinetic energy U of the beam must be dissipated in the sample, dU/dz is much larger near the end of the electron range, but the thick sample itself acts as a sufficiently good thermal sink in most cases to preclude objectionable temperature rises.

Atomic Displacements

The principal result of the inelastic interaction with nuclei, and indeed of most inelastic interactions with atomic electrons, is to increase the phonon spectrum through small energy transfers, i.e. to heat the specimen. This is a collective response of the atoms in a solid which relies on the fact that an atom is bound to its neighbors. An individual response is possible if the individual atom is given kinetic energy substantially more than its bonding energy, so that it is displaced to some normally unoccupied interstice in the structure, creating a Frenkel (interstitial, vacancy) pair of defects. The

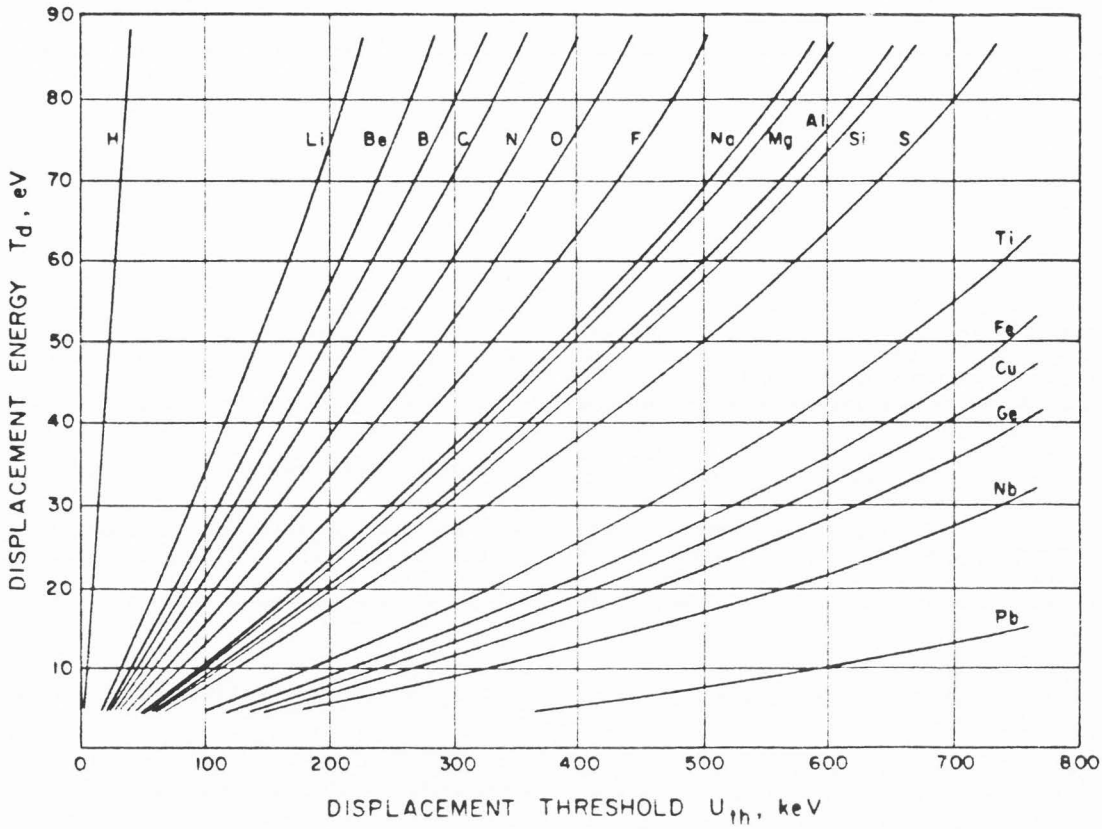

Fig. 3. Energy transferred in ballistic displacements as function of atomic species and electron energy.

displacement energy τ_d required depends on the strength of bonding in the solid, as well as the compactness of its structure, and varies from a few eV in semiconducting compounds and organic materials to tens of eV in compact ionic oxides.

The transfer of kinetic energy to the displaced atom may be direct or indirect. **Direct displacement** utilizes the kinetic energy and momentum transferred to a nucleus by the incident electron in a ballistic collision, sometimes called **knock-on** displacement after an obscure English blood sport. The maximum energy transferable

$$\tau^{max} = 2U(U + 2mc^2)/Mc^2 \qquad (20)$$

(which reduces to (4m/M)U for non-relativistic electrons, $U << mc^2 = 511$ keV) depends on the incident electron energy U, so there will be some threshold energy U_{th} above which $\tau^{max} > \tau_d$. U_{th} is plotted against τ_d in Fig. 3 to generate a series of displacement curves for each element. From these it can be seen that, for typical displacement energies τ_d in the 10-40 eV range, 200 keV electrons can directly displace many light elements in weakly-bonded solids, while 300-500 keV electrons can displace heavier atoms in even strongly-bonded solids like oxides. This result holds considerable import for use of the new generation of intermediate voltage electron microscopes (300-500 kV), particularly in high resolution and focused probe modes where electron current density is large.

The displacement probability is conveniently given by the displacement cross section (simplified below to the non-relativistic case)

$$\sigma_d = Z^2 (8\pi a_H^2 U_R^2)/(Mc^2 \tau_d) \simeq .70 Z/\tau_d \qquad (21)$$

where τ_d in the second equality above is expressed in electron volts and σ_d in barns (10^{-28} m^2). Displacement cross sections typically saturate at this value, in the 10-100 barn range, once above threshold, rendering estimates of displacement rates straightforward.

Atomic displacements attributable to the far more common electronic excitations derive from a configurational instability of the atom in its excited or ionized state. This **indirect** displacement process is call **radiolysis** and requires four criteria to be satisfied: the excitation must have energy comparable to displacement energy and remain localized for times (~1 ps) long enough for the heavy atom nucleus to respond mechanically, for which response there must exist an energy-to-momentum conversion mechanism. Most delocalized excitations, such as plasmons (the most probably inelastic loss) eventually decay to sufficiently localized single-electron valence band excited states (excitons), though in semiconductors these may still prove too diffuse for radiolysis, and in metals such excitations are delocalized too rapidly (in times < 1 fs) by conduction electrons to be of use. Displacement energies in ionic oxides are

generally much higher than available exciton energies (except at the surface), but a surprisingly large number of other inorganic compounds (halides, hydrides, azides, many sulfides, a few more covalent oxides, and almost anything explosive) satisfy all four criteria to varying degrees.

For compounds which do satisfy the first three criteria, the efficiency of the overall radiolytic process depends largely on the efficiency of the energy-to-momentum transfer mechanism, details of which are known only for two inorganic systems: alkali halides (Kabler and Williams, 1978) and SiO_2 (Hobbs and Pascucci, 1980). In both these systems, the primary excitation is a valence-band exciton localized to a single anion (halogen or oxygen p states) which prompts removal of the anion from its site, with consequent formation of molecular interstitial crowdion species. Fig. 4 illustrates, for example, a putative sequence for SiO_2 networks, whereby an oxygen atom is removed radiolytically from an Si-O-Si linkage and incorporated into an Si-O-O-Si molecular "peroxy" linkage. A similar mechanism probably operates in silicate glasses, and also in zeolites in which Al is partially substituted for Si and water is structurally incorporated; the incorporated water can additionally radiolyse to form disruptive H^+ and OH^- radical species (Treacy and Newsam, 1987).

A number of ionic oxides, notably oxides of titanium (Berger et al., 1987), are found to desorb oxygen strongly from their surfaces under electron irradiation, ostensibly by a process apparently involving instead localization of **multiple** hole states at single oxygen anion sites. These may be the result of cation core electron ionization followed by charge transfer to anion valence states and additional Auger electron emission (Knotek and Feibelman, 1978; Knotek, 1984). The anomalously positively-charged oxygen ion is then ejected from its anion site, at least at surfaces (where τ^d is smaller), a displacement mechanism known as a 'Coulomb explosion' and originally envisaged by Varley (1962) to explain bulk radiolysis of halides.

Efficiencies for radiolytic processes may be high, as large as $\zeta = 0.1$ or more for halides and many organic compounds utilizing valence excitations, $\zeta = 10^{-4}$ for silicates and the phthalocyanines once beloved of high-resolution microscopists, but rather smaller for electron-induced desorption processes in oxides, involving the less probable core excitations. The corresponding displacement cross sections are given by

$$\sigma_r = \zeta\ (dU/dz)/(N\ \tau_d^*) \simeq 7 \times 10^6\ \zeta\ /\tau_d^* \qquad (22)$$

where τ_d^* is the displacement energy for the atomic species in its **excited** state (which may be less than τ_d). Again, τ_d^* and σ_d are expressed in eV and barns respectively in the second equality above which is directly comparable to (11). The ratios of the two cross sections

$$\sigma_r/\sigma_d = 7 \times 10^5\ \zeta \qquad (23)$$

shows that radiolytic displacement processes will dominate ballistic displacement whenever $\zeta > 10^{-5}$ (which it is for halides, silicates and organics), and of course will always prevail for $U < U_{th}$. The

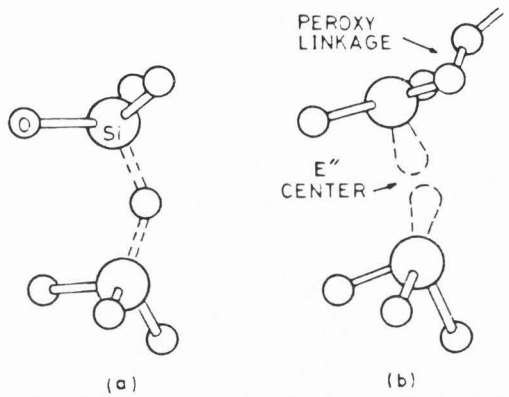

Fig. 4 Likely radiolysis sequence for SiO_2 and related network structures (Hobbs and Pascucci 1980).

presence of radiolysis can usually be confirmed by reducing the electron energy U to 40 keV or lower and comparing the damage rate to that at higher energies. At 40 keV, direct displacement is unlikely for all elements except hydrogen, and radiolysis is actually **more** efficient because of the (ln U)/U dependence of the energy loss rate in (12), almost all of which is attributable to electronic processes. Conversely, increasing U to 500 keV or more can more than halve the radiolysis rate from that at 100 keV, though at these energies ballistic displacements may begin to compete with the more efficient radiolysis process, and the elastic and inelastic scattering signals providing information are correspondingly diminished as well.

Specimen Degradation

The implications for displacement by either route are serious, perhaps not surprisingly considering the cataclysmic rate of energy deposition by electron probes. Table 2 indicates the displacement rates and fractions attending exposure to a flux of 10^5 electrons/nm^2·s for 10 s ($j = 10^4$ A/m^2), assuming $U > U_{th}$ for ballistic displacement and $\zeta = 0.1$ and 10^{-4} for radiolysis. This dose and dose rate correspond to those required for recording one high-resolution micrograph at atomic dimensions.

Table 2

Displacement rates and displacement fractions for one high-resolution micrograph

	$c_d(s^{-1})$	c_d
Ballistic displacement		
bulk	10^{-3}	10^{-2}
surface	10^{-2}	0.1
Radiolysis		
$\zeta = 0.1$ (halides, organics)	10	100
$\zeta = 10^{-4}$ (silicates)	10^{-2}	0.1

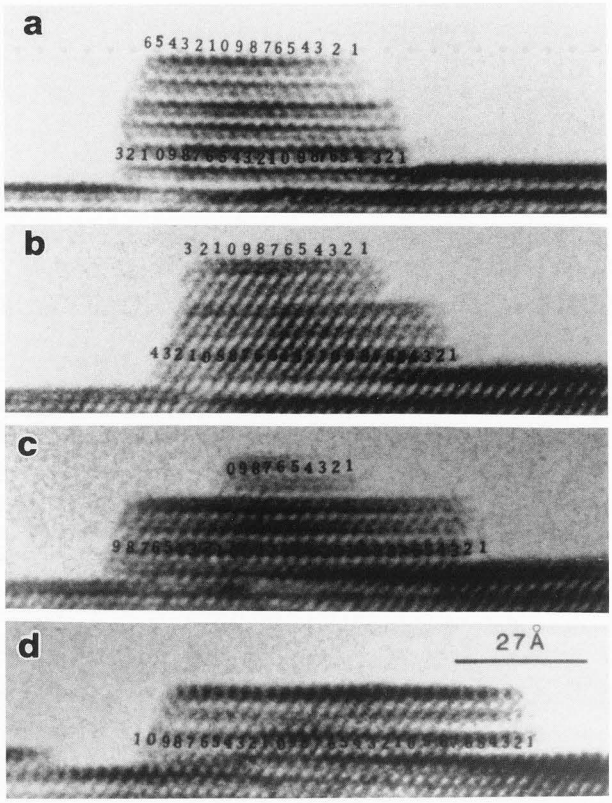

Fig. 5. Sequential profile images of β-PbO_2 surface irradiated with 200 keV electrons, showing progressive redistribution of surface atoms during high resolution TEM examination. (Kang and Eyring, 1987).

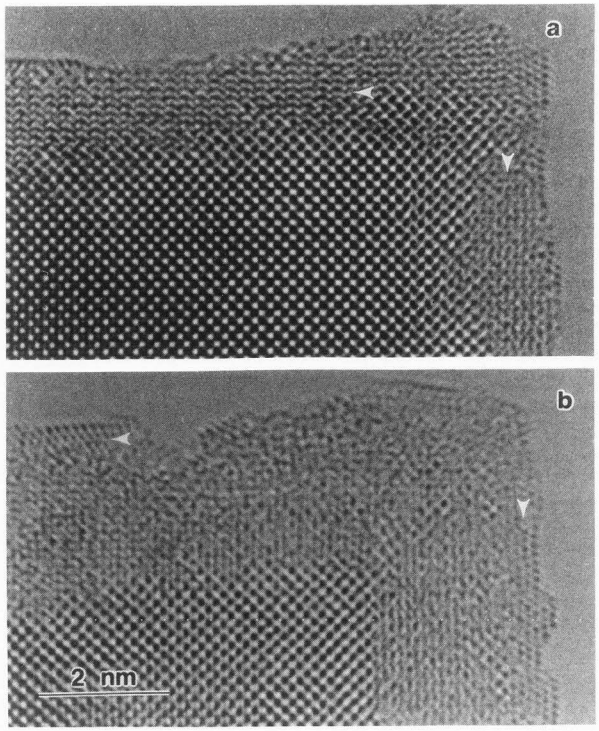

Fig. 6. Reduction of the surface region of a TiO_2 specimen to TiO via an intermediate phase (McCartney and Smith, 1989). Arrows mark altered phases.

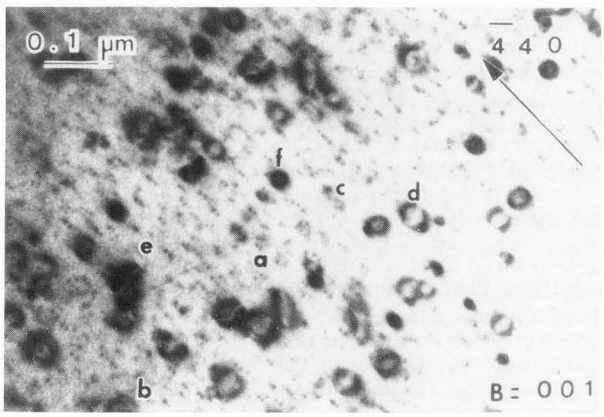

Fig. 7. Faulted dislocation loops formed in the ceramic magnesium aluminate spinel of approximate composition $MgAl_4O_7$ by 1 MeV electron irradiation. The fault plane is richer in Al than in the equilibrium composition $MgAl_2O_4$, and the loops effectively precipitate the excess Al. Letters a-f denote different equvalent loop orientations. (Parker, 1984).

Ballistic displacement levels of 10^{-2} displacements per atom (dpa) mean that, in the process of recording a single high-resolution image taken under conditions where direct displacement is possible (300-500 keV electrons for many materials), 1% of the atoms have been displaced, or one dis- placed atom occurs in **every** column of 100 atoms. The displacement of atoms associated with point defects, dislocation cores or surfaces, where τ_d is smaller, is 10-100 times more likely still. A surface displacement rate of 10^{-2} s^{-1} implies one monolayer removed every 100 s, or a tenth of the surface atoms rearranged in the recording of one image; such rates have particularly serious implications for the integrity of profile images of surfaces (Fig. 5).

The high displacement rates deriving from efficient valence-excitation-dominated radiolytic processes have still more serious implications. Where radiolysis is present, **every atom** may have been displaced as much as **100 times** during the recording of one high-resolution image! Electron-stimulated desorption of surface atoms usually occurs by less efficient radiolytic mechanisms (for example, those requiring initial core electron excitation which are far less probable than valence electron excitations). However, because the desorption may be ion-selective, surface chemistry may alter radically. This has been much studied in transition metal oxides which are successively reduced to lower oxygen content compounds (Fig. 6).

Radiation chemistry at the surface is strongly influenced by the local environment surrounding the specimen. Carbon contamination is the most ubiquitous example of irradiation-induced surface

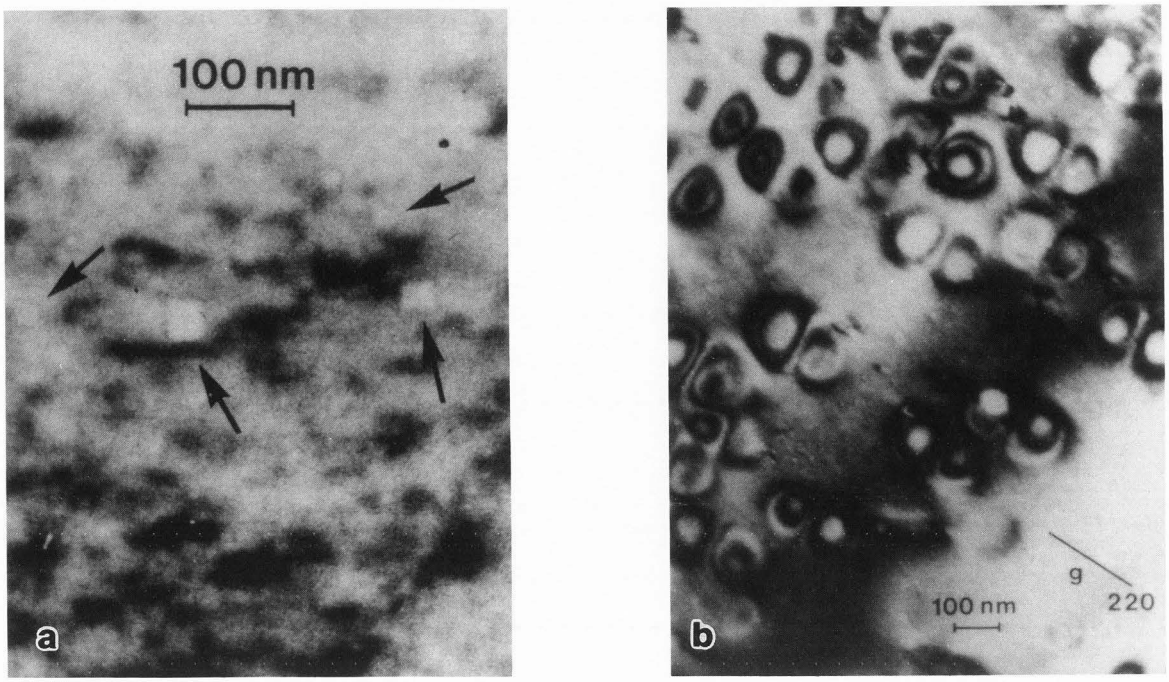

Fig. 8. Decomposition products of electron irradiation of halides. a) Cuboidal precipitates (arrowed) of Na metal in NaCl; b) chlorine bubbles in KCl. (Hobbs, 1976).

chemistry occurring in an electron beam; in this case, hydrocarbon contaminants in the microscope vacuum are radiolysed to an amorphous carbon or hydrocarbon glassy layer at the surface in times shorter than the persistence times for adsorbed hydrocarbon molecules. Hydrocarbon partial pressures in the range 10^{-6} torr (0.1 mPa), found in diffusion-pumped electron-beam instruments, yield contamination rates of the order of one monolayer/s (Hren, 1979). In cleaner ultrahigh-vacuum environments, it is more likely that any hydrocarbons present have been introduced with the specimen itself. Other common constituents of the instrument vacuum, O_2 and especially H_2O, can also react with the specimen surface in an ionizing environment. Radiolysis of water molecules yields particularly aggressive H^+ radicals. The chemistry attending such electron-beam induced surface reactivity is beyond the scope of this treatment and is discussed by Dresser (1990).

Sub-surface consequences of atomic displacement are less direct but can be no less dramatic, particularly at radiolytic displacement rates. Since few atoms leave the specimen interior as a result of primary displacement processes, what is important are the secondary responses of the solid to these displaced atoms. Whether meaningful information about structure (or even composition) can be extracted from a specimen when large numbers of atoms are being moved around internally by displacive mechanisms depends largely on the ability of the solid to police its short- and long-range order effectively. This ability varies markedly for different classes of solids, which can be grouped roughly as either compact, network or molecular. The Coulomb field in strongly ionic compounds, which form compact solids, is, for example, so effective in restoring order that lattice images of halides may be recorded (Yada and Hibi, 1969) even though every halogen is being displaced radiolytically more than ten times each second. Such dynamic images are really maps of the average Coulomb field rather than atomic structure images.

Structural redundancy is also a feature of compact solids, which include metals as well as ionic crystals, where high atomic coordination militates against loss of structural order. These solids tend to isolate damage by aggregating displaced atoms into extended defects (such as dislocations or precipitates of altered composition, Fig. 7), leaving the intervening material structurally unaltered. Atoms displaced to interstitial positions (interstitials) are mobile in most solids down to cryogenic temperatures, but at or somewhat above room temperature the vacant sites from which the atoms were displaced (vacancies) can also diffuse. In monatomic solids, their aggregation results in voids forming; but in compounds, aggregation of vacancies of one species results in precipitation of elemental or compound phases of the other remaining species. In this way, aggregation of halogen vacancies in electron-irradiated alkali halides results in precipitation of alkali metal particles (Fig. 8a).

Solids in which displaced atoms can form molecular species, e.g. halogen molecules in halides, O_2 in oxides, CO_2 in carbonates, H_2 in hydrocarbons, etc. can precipitate these species in condensed or gaseous form. Fig. 8b shows molecular chlorine inclusions (bubbles) in electron-irradiated KCl; similar oxygen bubbles are generated in electron-irradiated silicate glasses (De Natale and

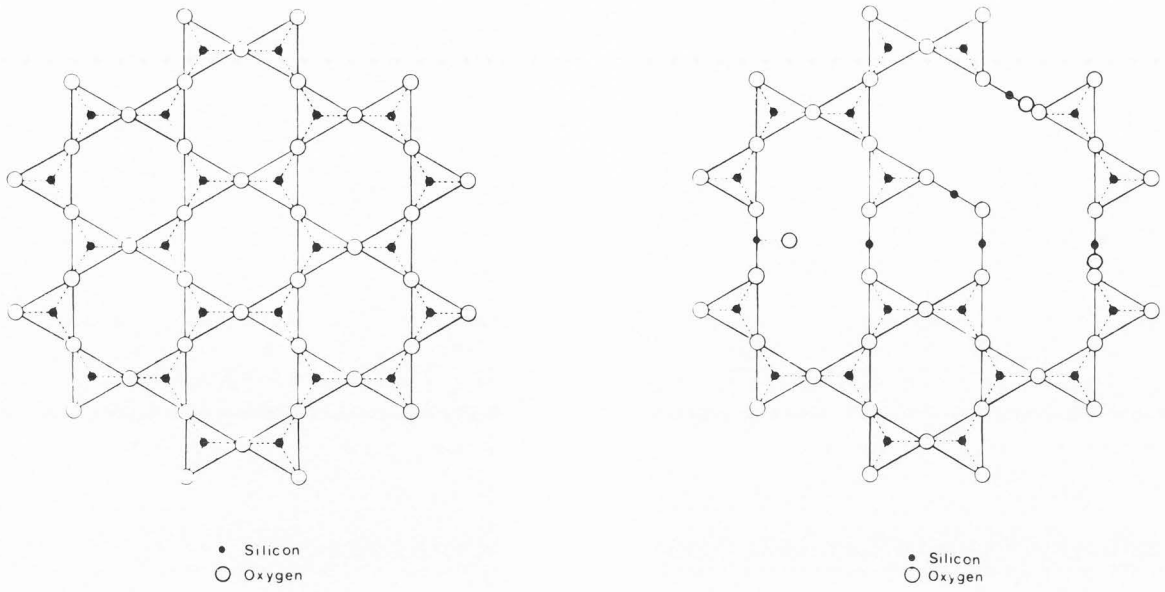

Fig. 9. Projected schematic sequence leading to incipient structural collapse of an SiO_2 tetrahedral network in which a critical density of broken Si-O-Si linkages (and peroxy linkages created) accumulates.

Howitt, 1984). Both forms of elemental precipitation signal progressive decomposition of specimen material, though usually heterogeneously with large intervening regions remaining undecomposed.

Covalent solids, with shorter-range directed bonding and lower coordination, are less effectively policed and are likely to lose long-range correlations. These solids commonly form more open network structures which, when initially crystalline and structurally disordered, revert to amorphous (or, more precisely, aperiodic) glasses. Quartz and most silicates (like zeolites) exhibit this response, as do all organic solids. Fig. 9 shows schematically how structural collapse could attend accumulation of a critical density of eliminated Si-O-Si linkages in SiO_2 during radiolysis. Such transformations are generally stochastic and irreversible. Their onset marks an end to extractable structural information, because no unambiguous structural information about aperiodic structures can currently be derived from diffraction or images modes of the electron microscope (Liu et al., 1988). Optical diffractogram analysis from images of areas in transition can provide some information about the structural changes occurring during the amorphization process (Pascucci et al., 1983).

Molecular solids are characterized by strongly-bonded molecular units bound more weakly to other such units. Ice and simple organic molecular crystals like mothballs (naphthalene) are classic examples; polymers and crystalline proteins more complex ones. Two sorts of degradation are possible in such solids: chemical alteration of the molecular unit through loss, addition or rearrangement of atoms; and attendant structural relaxations of the molecule positions. The topology of such solids is based on steric consideration which provide only poor policing of long-range structural order, so altering the molecular unit provides added structural freedoms. Altered molecules can react with and bond chemically to neighboring molecules, further compromising both chemical and structural integrity (Reimer, 1984). In addition, atoms displaced by irradiation often depart in gaseous combinations, such as H_2, H_2O, NH_3, CO, CO_2, S_2, SiH_4, SiO etc., leading to substantial mass loss (as much as 50% or more!) and gross morphological changes such as bending, buckling or shrinkage of the sample. Simple point-defect-like alterations are therefore catalytic and initiate far-reaching structural consequences. The most readily observable consequence is that crystalline arrangements inexorably lose their long-range correlations under irradiation, just as do many network solids.

Organic molecular solids damage predominantly by radiolysis, though the mechanism clearly depends on the nature of the internal molecular bonding (Isaacson, 1975). In non-conjugated aliphatic hydrocarbons, radiolysis appears to be dominated by valence electron excitations which lead to scissioning of C-C and C-H bonds with high efficiency ($\zeta > 0.1$). The π-bonding in aromatics is effective in delocalizing valence excitations, and aromatic compounds instead exhibit a threshold for damage at 284 eV corresponding to carbon K-shell ionization (Mohd Muhid et al., 1988). The damage mechanism likely involves a Knotek-Feibelman-like multiple ionization and ejection of a carbon atom following Auger decay of the initial core hole. The bonding redundancy is very important: graphite and diamond, in which the identical C K-shell excitations and Auger-induced multiple ionizations no doubt occur, are exceptionally beam-stable because every carbon atom is bonded to two other or three others respectively; in organic molecules, many carbon atoms are bound to only two or even one other carbon. Scissioned products also play an

important role. A liberated hydrogen ion (a bare proton!) is a particularly aggressive and reactive radical species, capable of inflicting chemical damage elsewhere in the same or adjacent molecules.

Palliative Measures

The irradiation-induced chemical and structural alterations cited above define a perverse Uncertainty Principle for electron probes, by which the more information one collects about the specimen the less reliable is that information. The ontological essence of this dilemma may be subsumed succinctly into a universal verity I shall dub the **Uncertainty Principle according to Murphy**

"The more you look, the less you see." (24)

Assuming that the specimen is not being examined in order to investigate its irradiation response, it is necessary to decide at what point the information being collected is no longer representative of the object being examined. This critical point, which in turn depends on the scale of information sought, sets the resolution limit of the information available due to the Poisson statistical consideration (6). Three palliative options are available to the practitioner faced with the dilemma (24): 1) eliminate, or reduce the efficiency of, the displacement mechanisms; 2) minimize the secondary structural responses to irradiation-induced disorder; 3) maximize the **recorded** information from each incident electron.

Sub-surface ballistic displacements can be avoided by reducing electron energy U below the displacement threshold, though displacements at the surface are likely to occur even at half the bulk displacement threshold, or less. Also, many instruments are unlikely to perform optimally at lower accelerating voltages; the current generation of 300-400 kV TEMs are a case in point and function poorly at 100-200 kV for high resolution. Where radiolysis dominates, high electron energies (200 keV to 1 MeV) reduce the **inelastic** scattering cross sections, by as much as a factor of 2-3 over 50-100 keV; the **elastic** cross section is, unfortunately, correspondingly reduced, which can negate any advantage for certain imaging modes. Some, but not all, radiolysis mechanisms are temperature dependent, and cooling of the specimen to cryogenic temperatures may reduce the primary displacement rate in such cases.

Generally, more advantage can be obtained from manipulating the **secondary** responses, which influence the **kinetics** of damage accumulation. The fate of the overwhelming majority of newly created displaced atoms is simply to return to vacated atom sites; such recombination is termed **geminate** if the displaced atom returns to the **same** vacancy that it created, and **non-geminate** if it recombines with a previously vacated site. Non-geminate recombination can occur **athermally** through the simple statistical distribution of primary damage sites: a new displacement just happens to be created next to an existing vacancy, the probability for which will increase with defect content. Also, once a local volume of material has been damaged by secondary responses (e.g. chemical alteration, amorphization),

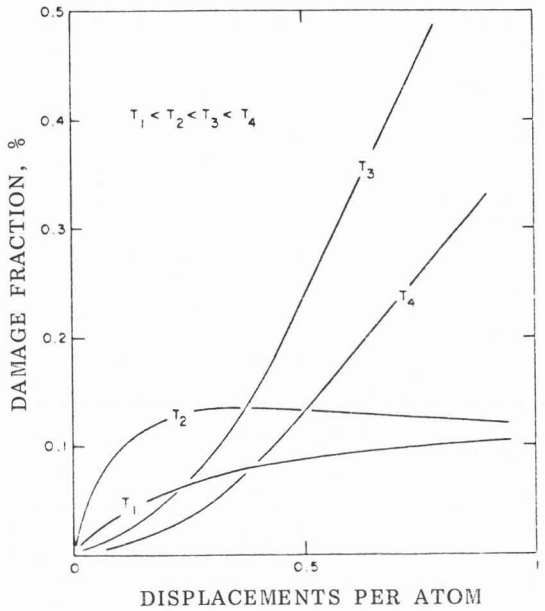

Fig. 10. Defect accumulation kinetics characteristic of four irradiation temperatures T1 < T2 < T3 < T4: T1, the lowest temperature, where neither vacancies nor interstitials are mobile and reach sinks; T2 where only interstitials reach sinks; T3 where all effects reach sinks and non-geminate athermal recombination is minimal; T4 where sinks begin to lose stability at higher temperature.

it may not be possible (or germane to consider) further damage to that volume, and as such volumes accumulate, there will be progressive exhaustion of undamaged material available to damage, which likewise reduces the rate of stable damage production. Both considerations can be incorporated into a differential rate equation of the form (Hobbs, 1984)

$$dc/dD = G\,(1 - c^{m'}) - R(c) \qquad (25)$$

where G represents the forward rate of primary damage events, c the defective fraction at a given dose D, R is the recombination rate and $m' \neq 1$ allows for possible cooperative effects (e.g. multiple damage events in the same local volume required for a secondary response).

For $m' = 1$ and $R = 0$ or $R = R'(1 - c)$, (25) integrates to saturating kinetics of the form

$$c = 1 - \exp(-G'\,D) \qquad (26)$$

with $G' = G - R'$. Inclusion of any significant restorative term (R(c) which increases with defect content

$$R(c) = R''c, \qquad (27)$$

which is the case for non-geminate athermal recombination, leads to saturating kinetics at doses and damage fraction far below those encountered due to exhaustion of undamaged materials, as represented

by (26). An approximate solution to (25) leads in this case to accumulation at a rate

$$c \simeq (1/4\omega)\ \ln(4\omega\ G'\ D) \qquad (28)$$

where G' is the production rate of defects surviving geminate recombination and ω is the **athermal recombination volume** within which creation of a complementary defect will result in spontaneous recombination. For compact solids, spontaneous recombination takes place with vacancy-interstitial separations ≤ 5 atom sites, implying $\omega \simeq 1000$ atomic volumes; the rate of defect accumulation dc/dD is accordingly reduced to a tenth of its initial value at a defect fraction $c \simeq 10^{-3}$ (curve T1, Fig. 10). If defects are mobile, as typically occurs at higher temperatures, the situation actually becomes **worse**, because defects can accumulate at sinks, such as dislocation loops, voids, precipitates, bubbles, etc., in which their individual recombination volumes substantially overlap, with the probability of non-geminate athermal recombination decreasing sharply. If aggregation occurs for only **one** defect species (for example, interstitials but not vacancies), the **rate** of defect accumulation increases by a factor of about 4 (curve T2, Fig. 10), while if stable sinks exist for **both** species (T3, Fig. 10)

$$dc/dD \simeq G' \qquad (29)$$

and the accumulation is linear to much higher defect content, limited only by exhaustion again as described by (26). Irreversible secondary responses (such as dimerization of adjacent damaged molecules in molecular solids) represent sinks in this sense, as does the surface when mobile displaced atoms escape to or beyond it. In compact and network solids, it may appear that the very thinnest regions in a TEM image remain damage-free, because no aggregate sinks form in deference to the surface, which is the more effective local defect sink; however, if the displaced atoms drawn to the surface remain there, the surface is being continually reconstructed with linear kinetics (29).

Where little care is taken to provide adequate heat sinks, electron-beam heating can catapult specimens into the temperature range where linear kinetics (29) rapidly erode a significant fraction of the irradiated material. Conversely, cryogenic temperatures can establish kinetics more like (28); temperatures below 10-20 K may, however, be required to halt interstitial mobility altogether in compact solids (Hobbs, 1974). In molecular solids, low temperature may effectively freeze damaged molecular units in place and retard secondary responses (so-called "cage effect") or reduce mobility of active radical species such as H^+. Regrettably, temperature appears to have little effect on amorphization of network structures, such as quartz (Pascucci et al., 1983), where the coordination units are smaller and secondary restructuring easier than for molecular solids.

Comparatively little attention has been given to maximizing the **recorded** information from each electron, apart from practice of "minimum dose" techniques which minimize the "dead time" exposure when actual recording is not being carried out. Photographic emulsions are almost exclusively used for recording electrons in TEM and can be optimized (Valentine, 1965), though seldom are, for a given allowable specimen dose. Scanning is a potentially more effective method for imposing a controlled electron dose, but electron detectors are presently less efficient than photographic emulsions. With periodic samples, signal averaging the information from identical repeated units is an effective way to best the otherwise immutable Poisson statistics and has provided nearly atomic-scale images of protein structure (Unwin and Henderson, 1975). Reconstruction from noisy images by sophisticated computer methods, such as maximum entropy approaches (Anderson et al., 1989), is still in its infancy.

Conclusion

It is important in obtaining structural or analytical information from fast electron probes to understand fundamentally how and why a specimen could have altered during examination. Specimen heating is largely a matter of providing adequate heat sinks. The external and most internal consequences of charge acquisition can be obviated by application of thin conducting films. Ballistic displacement of atoms occurs only for electron energies above threshold, which need not be exceeded in most cases, though it is difficult not to displace surface atoms at practical electron energies. The resulting defect generation rates are marginally unacceptable only for the highest resolution work, and in the worst cases (light, weakly-bound atoms) radiolytic displacement mechanisms often instead dominate. Specimen degradation is usually the result of secondary responses to initial displacements, which can be ameliorated to some extent by manipulation of degradation kinetics, application of cryogenic temperatures, and intelligent utilization of observation and recording media and the necessarily incomplete information they register.

Acknowledgment

The author is grateful for the U.S. Department of Energy for research support during the period when this research and its present elaboration were being carried out, and the Massachusetts Institute of Technology for a travel award.

References

Anderson DM, Martin DC, Thomas EL. (1989) Maximum-Entropy data resolution using both real- and Fourier-space analysis. **Acta Cryst. A45**, 686-698.

Berger SD, Macaulay JM, Brown LM. (1987) Radiation damage in TiO_x at high curent density. **Phil. Mag. Lett. 56**, 179-185.

Cazaux J, Le Gressus C. (1991) Phenomena related to charge in insulators: Macroscopic effects and microscopic causes. **Scanning Microscopy** (to be published).

De Natale JF, Howitt DG. (1984) A mechanism for radiation damage in silicate glasses. **Nucl. Instrum. Methods in Phys. Res., B1**, 489-497.

Dresser MJ. (1990) Electron stimulated surface chemistry. **Scanning Microscopy Supplement, 4.**

Hobbs LW. (1974) Transmission electron

microscopy of defects in alkali halide crystals. **Surface and Defect Properties of Solids**, Vol. 4, ed. MW Roberts, JM Thomas (The Chemical Society, London), 152-250.

Hobbs LW. (1976) Point defect stabilization in ionic crystals at high defect concentrations. **J. Physique 37** (Colloque C7), 1-26.

Hobbs LW, Pascucci MR. (1980) Radiolysis and defect structure in electron-irradiated alpha-quartz. **J. Physique 41**, (Colloque C6), 237-242.

Hobbs LW. (1984) Radiation effects in analysis by TEM in **Quantitive Electron Microscopy**, ed. JN Chapman and AJ Craven (Scottish Universities Summer Schools in Physics Publications, Edinburgh), 399-445.

Hren JJ. (1979) Barriers to AEM: Contamination and etching in **Introduction to Analytical Electron Microscopy**, ed. JJ Hren, JI Goldstein, DC Joy (Plenum Press, New York), 481-505.

Isaacson M. (1975) Inelastic scattering and beam damage in biological molecules in **Physical Aspects of Electron Microscopy and Microbeam Analysis**, ed. BM Siegel, DR Beaman (Wiley, New York), 247-258.

Kabler MN, Williams RT. (1978) Vacancy-interstitial pair production via electron-hole recombination in halide crystals. **Physical Rev. B18**, 1948-1960.

Kang ZC, Eyring L. (1987) Surface processes observed by high resolution electron microscopy: beam induced transformation and reduction in a modified β-PbO_2 crystal. **Ultramicroscopy 23**, 275-282.

Knotek ML, Feibelman PJ. (1978) Ion desorption by Core-hole Auger decay. **Phys. Rev. Letters 40**, 964-967.

Knotek ML. (1984) Stimulated desorption. **Rep. Prog. Phys. 47**, 1499-1561.

Kohl H. (1990) Spatially sensitive energy loss spectroscopy. **Scanning Microscopy Supplement, 4.**

Liu ZQ, McKenzie DR, Cockayne DJH, Dwarte DM. (1988) Electron diffraction study of the structure of boron- and phosphorus-doped hydrogenated amorphous silicon. **Phil. Mag. B57**, 753-761.

McCartney R, Smith DJ. (1989) Epitaxial relationships in electron-stimulated desorption processes at transition metal oxide surfaces. **Surface Science, 221**, 214-232.

Mohd Muhid MN, Howie A, Rocca FJ, Valdre U. (1988) Electron beam damage in organic materials. **Proc. IV Asia Pacific Conference and Workshop on Electron Microscopy** (Bankok, Thailand), 327-334.

Mott NF, Massey HSW. (1965), **Theory of Atomic Collisions** (Oxford University Press, Oxford).

Murphy E. (1949) Edward Murphy was an American development engineer who, exasperated with a laboratory technician's chronic disposition to error, lamented "If there is any way to do it wrong, he will". The complaint was quickly generalized to (4). A fuller biographical account can be found in the article by Dianna Waggoner entitled "Murphy's Law really works, and nobody knows it better than Murphy, the unsung sage of the screw-up" in **People Weekly, Vol. 19** (31 January 1983) p. 81. A much earlier statement of its consequences is the rendition in verse by 19th-century poet James Payn:

"I never had a piece of toast
Particularly long and wide
But fell upon the sanded floor
And always on the buttered side."

Parker CA. (1984) Fast neutron and electron irradiation damage in magnesium aluminate and aluminum oxynitriode spinels. **PhD Thesis,** Massachusetts Intitute of Technology, Cambridge, MA.

Pascucci MR, Hutchison JR, Hobbs LW. (1983) The metamict transformation in alpha-quartz. **Rad. Effects 74**, 219-226.

Reimer L. (1984) Methods of detection of radiation damage in electron microscopy. **Ultramicroscopy 14**, 291-303.

Rose A. (1948) Television pickup tubes and the problem of vision. **Adv. Electronics 1**, 131-166.

Schou J. (1988) Secondary electron emission from solids by electron and proton bombardment. **Scanning Microscopy 2**, 607-632.

Spencer LV. (1959) Energy dissipation by fast electrons, **National Bureau of Standards Monograph 1** (NBS, Washington, DC).

Treacy MMJ, Newsam JM. (1987) Electron beam sensitivity of zeolite L. **Ultramicroscopy 23**, 411-420.

Unwin PNT, Henderson R. (1975) Molecular structure determination by electron microscopy of unstained crystalline specimens. J. Mol. Biol. **94(3)**, 425-440.

Valentine RC. (1966) Response of photographic emulsions to electrons. **Adv. Opt. Electron Microscopy 1**, 180-203.

Varley JHO. (1962) Discussion of some mechanisms of F-centre formation in alkali halides. **J. Phys. Chem. Solids 23**, 985-1005.

Whiddington R. (1914) The transmission of cathode rays through matter. Proc. Roy. Soc. **A89**, 554-560.

Yada K, Hibi T. (1969) Fine lattice fringes around 1 Å resolved by axial illumination. **J. Electron Microscopy 18**, 266-271.

Editor's Note: All of the reviewer's concerns were appropriately addressed by text changes, hence there is no Discussion with Reviewers.